SolarPACES 2022, 28th International Conference on Concentrating Solar Power and Chemical Energy Systems
Analysis and Simulation of CSP and Hybridized Systems
https://doi.org/10.52825/solarpaces.v1i.885
© Authors. This work is licensed under a Creative Commons Attribution 4.0 International License
Published: 01 Mar. 2024

A Real-Time Capable Simulation of Open Volumetric Receiver Surface Temperatures with Spatially High Resolution

Kevin Iding[1,2][https://orcid.org/0000-0001-7968-5134], David Zanger[1,2][https://orcid.org/0000-0002-6111-7531], Daniel Maldonado Quinto[1][https://orcid.org/0000-0003-2929-8667], and Robert Pitz-Paal[1,2][https://orcid.org/ 0000-0002-3542-3391]

[1] Institute of Solar Research, German Aerospace Center (DLR), Germany

[2] Chair of Solar Technology, RWTH Aachen University, Germany

Abstract. The performance of open volumetric receivers can profit from advanced control of the heliostat aim points and the air mass flow. Advanced control techniques like model predictive control and state observer are based on dynamic system models. A suitable model for this purpose is introduced and validated with data recorded at the solar tower Jülich. The model shows good performance with respect to the dynamics of individual absorber cups. The simulation of the whole receiver requires an advanced optimization of the model parameters.

Keywords: Open Volumetric Receiver, Solar Tower, Simulation

1. Introduction

The surface temperature, its gradients, and transients determine the operational limits of solar thermal receivers. For convenience, these quantities are translated into allowable flux densities that may be supplied by the heliostat field. The allowable flux density is typically calculated in advance as a function of the heat transfer fluid mass flow under steady state conditions. Control strategies for the heliostat field consequently focus on maintaining these flux limits while minimizing spillage losses to increase the plant efficiency, assuming a steady state of the receiver.

The mass flow controller of the receiver, on the other hand, tries to achieve the desired outlet temperature while considering changes in the incident solar power as disturbances. While closed-loop mass flow controllers are state of the art, closed-loop control of the heliostat field is still under development [1]. This is due to the large number of aim points to be controlled and the difficulty of measuring the solar flux density at the receiver surface [2].

In control theory, a state estimator is a well-known concept for determining quantities that are difficult or impossible to measure. Therefore, we propose using a state estimator instead of relying on the solar flux density measurement or ray tracing. The state estimator can incorporate various measurements and simulations of quantities - such as flux density, surface temperature and output temperature - to determine a more reliable system state. However, this requires a sufficiently accurate and fast model of the receiver. Since the model would have to predict the thermal behavior of the receiver, this would provide an additional opportunity to overcome the steady-state limits of the allowable flux density. Instead the temperature limits at the receiver surface can be used as constraints for the aim point control. This is particularly useful for controlling transient conditions such as clouds, where a static allowable flux density

is not appropriate. This contribution focuses on developing and verifying a suitable model which can be used for a state estimator or an enhanced aim point control strategy.

2. Dynamic Receiver Model

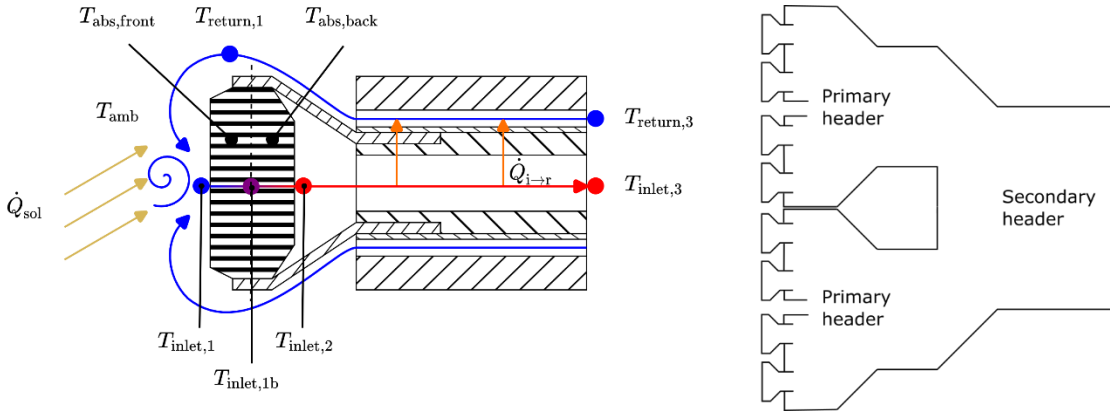


Figure 1. Single absorber cup (left) and absorber cups and headers (right).

2.1 Receiver Design

This work models the open volumetric receiver at the solar tower in Jülich and is based on the model developed by Jan Gall [3]. The receiver front consists of individual absorber cups. These absorber cups are divided into four sectors. Each sector has its own header element, which mixes the air flowing through the cups to homogenize the temperature. After mixing in the four primary headers, the resulting air flows are further combined in a secondary header. The out flowing air from the secondary header is then directed to either the heat storage or the power block and cooled down. The temperature remains significantly above ambient levels. Consequently the air is rerouted to the receiver and blown through gaps between the absorber cups in front of the receiver, to recover some of the remaining thermal energy.

To develop a fast dynamic model, the model is greatly simplified using the following assumptions: 1. Only temperatures are used as state variables. 2. A constant pressure is assumed (isobaric). 3. Heat transfer occurs exclusively within a cup and not between neighboring cups. 4. The air temperature within balance spaces is uniform and changes discretely at the boundaries of these spaces. 5. The absorber comb is the only component that stores thermal energy.

To model the receiver, the receiver is divided into the absorber cups and the headers.

2.2 Absorber Cup

A single absorber consists of three components: a comb structure that provides a large heat transfer surface, a funnel that collects the air behind the comb, and a piece of tubing. The absorber comb is a porous ceramic structure that absorbs the concentrated solar radiation, converts it into thermal energy, and stores it as internal energy. The air flowing through the porous structure acts as a heat transfer medium. It absorbs the energy, transferred by the ceramic and transports it through the air circuit. The funnel has roughly the shape of a truncated pyramid with a square base and a round outlet. It is solid and made of the same material as the comb. The tubing incorporates the end piece of the funnel, some insulation and a steel pipe. This structure must be adequately considered when calculating the heat transmission. From the cylindrical tube, the air flows into the headers.

2.3 Energy balances

Fig. 1 illustrates the energy balances of a single absorber. The absorber cup is discretized into a heating zone and a transport zone. The heating zone represents the absorber comb which absorbs the solar irradiation. The transport zone consists of the absorber tub and the two pipe sections. It would also be possible to treat each part as an individual balance space. However, since the temperature does not change along these components, one balance space combines these three parts.

Since the absorber surface heats up faster than the back, the comb is discretized into two parts. The front part and the back part. The energy balance around the front part (see Fig. 1) yields the following equation

$$\dot{U}_{abs,front} = \dot{Q}_{sol} - \dot{Q}_{loss,\ conv} - \dot{Q}_{loss,rad} - \dot{Q}_{comb,front} - \dot{Q}_{cond} \tag{1}$$

Here, $\dot{U}_{\mathrm{abs,front}}$ describes the change in internal energy of the comb, $\dot{Q}_{comb,front}$ the heat transfer between the absorber comb and the incoming air and $\dot{Q}_{sol}$ the solar irradiation absorbed by the comb. The loss terms $\dot{Q}_{loss,conv}$ and $\dot{Q}_{loss,rad}$ represent the thermal loss due to wind and radiation respectively. $\dot{Q}_{cond}$ considers the conductive heat transfer to the back comb. The internal energy rate can be expressed as

$$\dot{U}_{abs} = m_{abs} c_{abs} \frac{dT_{abs}}{dt} \tag{2}$$

with m_{abs} and c_{abs} describing the absorber mass and heat capacity respectively.

$$\dot{Q}_{sol} = \xi_{sol}\ \alpha_{sol} P_{sol} = \xi_{sol} \alpha_{sol} A_{abs} F \tag{3}$$

Where ξ_{sol} is the fraction of the total absorbed energy absorbed by the front part of the comb. Correspondingly $(1 - \xi_{sol})$ is the fraction which is absorbed in the back part. The amount depends on the comb geometry of the comb and the angle of incidence of the concentrated sunlight. On the other hand, α_{sol} is material dependent and denotes the absorption coefficient. The quantity F is the flux density and multiplied by the absorber front surface A_{abs} results in the solar power P_{sol}. The loss due to convection $\dot{Q}_{loss,conv}$ cannot be clearly distinguished from a low air return ratio which is described below, as the air in front of the receiver is sucked into it. Furthermore, modelling of wind disturbance and its influence on convective heat losses and the air return ratio is highly complex and subject to current research. Consequently, the convective loss is set to zero and only implicitly considered within the air return ratio.

The loss due to the radiation of the hot absorber cup can be described by the Stefan-Boltzmann law

$$\dot{Q}_{loss,rad} = \epsilon \sigma A_{abs} \left(T^4_{abs,front} - T^4_{amb} \right) \tag{4}$$

with the Stefan-Boltzmann constant σ and the ambient temperature T_{amb} . To keep the model simple α_{sol} and emission coefficient ϵ are set equally.

Furthermore, $\dot{Q}_{comb,front}$ can be written as the differences of the enthalpy of the incoming air with $T_{inlet,1}$ and the air leaving the front comb with $T_{inlet,1b}$.

$$\begin{aligned} \dot{Q}_{comb,front} &= \dot{H}_{inlet,1b} - \dot{H}_{inlet,1} \\ &= \dot{m}_{abs} \cdot \left(h_{inlet,1b} - h_{inlet\ ,1} \right) = \alpha_{comb,front}\ A_{comb,front} \left(T_{abs,front} - T_{m,front} \right), \end{aligned} \tag{5}$$

where $\alpha_{comb,front}$ is the heat transfer coefficient and $A_{comb,front}$ is the contact area between the absorber comb and air. The convective air temperature is calculated from the incoming $T_{\text{inlet},1}$ and outgoing $T_{\text{inlet},1b}$ air temperature by

$$T_{m,front}=\left(1-w_{T,front}\right)T_{inlet,1}+w_{T,back}T_{inlet,1b} \tag{6}$$

$w_{T,front}$ represents an adjustable parameter. Finally, $\dot{Q}_{cond}$ can be expressed by

$$\dot{Q}_{cond}=\lambda_{comb}\cdot\frac{A_{solid}\cdot\left(T_{abs,front}-T_{abs,back}\right)}{l_{comb}/2} \tag{7}$$

Where A_{solid} is the solid surface area between front and back l_{comb} the depth of the absorber and λ_{comb} is the heat conduction coefficient of the ceramic.

$T_{inlet\ ,1}$ can be derived from an energy balance around the air in front of the comb (see Fig. 1).

$$H_{inlet\ ,1}=arr\cdot h_{return,1}+(1-arr)\cdot h_{amb} \tag{8}$$

where *arr* is the air return ratio, which indicates the fraction of returned air that flows back into the absorber. One could also rewrite the specific enthalpy as the product of the heat capacity and the temperature $h=c_p(T)T$. However, to save computational costs the function $h(T)$ and its inverse $T(h)$ is approximated by a third-order polynomial for all air streams.

Analogously, the equations for $T_{abs,back}$ can be derived. However, for the back no radiation loss is considered. The new unknown $h_{return,1}$ can be calculated from energy balances around the transport zone.

2.4 Transport Zone

The energy balance around the transport zone of the returned air (see Fig. 1) yields

$$\dot{m}_{abs}h_{return,1}=\dot{m}_{abs}h_{return,\ 2}+\dot{Q}_{loss,i\rightarrow r} \tag{9}$$

Here, $\dot{Q}_{loss,i\rightarrow r}$ is the heat flow from the hot inlet air to the return air, which is described by

$$\dot{Q}_{loss,i\rightarrow r}=\alpha_{i\rightarrow r}\cdot A_{i\rightarrow r}\cdot\left(T_{inlet,2}-T_{return,3}\right) \tag{10}$$

where $\alpha_{i\rightarrow r}$ is the heat transfer coefficient and $A_{i\rightarrow r}$ the corresponding area for the heat transfer. To reduce computational costs the coefficient $\alpha_{i\rightarrow r}$ is approximated by a third-order polynomial fitted to a detailed model of the radial heat transfer through the pipe and insulation and using the Nusselt correlation for annular gaps and pipes. The polynomial depends only on the mass flow and the inlet temperature $T_{inlet\ ,2}$. Thus, the polynomial does not depend on the temperature $T_{return,3}$ as it was found to have a rather small influence in the considered operating temperature range.

The temperature of the return air $T_{return,3}$ is a measured variable in the power plant and therefore known. The last unknowns are $T_{inlet,1b}$ and $\mathrm{T_{inlet,2}}$, which can be derived from an energy balance around the air in the absorber comb

$$0=\dot{m}_{abs}\left(h_{inlet,1}-h_{inlet,1b}\right)+\dot{Q}_{comb,front} \tag{11}$$

$$0=\dot{m}_{abs}\left(h_{inlet,1b}-h_{inlet,2}\right)+\dot{Q}_{comb,back} \tag{12}$$

Combining all the stated equations results in a differential-algebraic equation system with two ordinary differential equations and two algebraic equations. With $T_{abs,\ front}$ and $T_{abs,\ back}$ as the

states, and $T_{inlet,1b}$ and $T_{inlet,2}$ as the algebraic variables. When solving this system, the outgoing air temperature $T_{inlet,3}$ can be calculated by an energy balance around the transport zone of the inlet air by

$$h_{inlet,3} = h_{inlet,2} - \frac{\dot{Q}_{loss,i \to r}}{\dot{m}_{abs}} \tag{13}$$

The temperature $T_{inlet,3}$ can then be calculated from the inverse function $T(h)$.

With all these equations, the whole absorber cup is defined. To compute the output for an array of absorber cups each output can be calculated individually. To increase the performance, the output of the individual cups can be computed in parallel. The output temperature $T_{inlet,3}$ is then used in the equations for the header modules.

2.5 Header

The outflowing air of each cup is mixed in one of the four primary headers. Each primary header has a rectangular form and takes the air from the same amount of absorber cups. The enthalpy of the mixture is given by

$$\dot{H}_{inlet,3,mixed} = \sum_i \dot{m}_{abs,i} \cdot h_{inlet,3,I} \tag{14}$$

The enthalpy flow of the outflowing air can be derived from an energy balance around the header, given by

$$\dot{H}_{inlet,4} = \dot{H}_{inlet,3,mixed} + \dot{Q}_{loss,header,1} \tag{15}$$

with $\dot{Q}_{loss,\ header,1}$ being the heat losses through the header walls, given by

$$\dot{Q}_{loss,header,1} = \alpha_{header,1} \cdot A_{header,1} \cdot \left(T_{inlet,3,mixed} - T_{amb}\right). \tag{16}$$

With the heat transfer coefficient $\alpha_{header,1}$ and the respective heat transfer surface $A_{header,1}$. $\alpha_{header,1}$ is calculated by converting the funnel-shaped header into an equivalent cylindrical shape. The equations for the secondary header can be derived analogously. The resulting energy balances yield an equation for the output temperature of the whole receiver $T_{inlet,5}$.

The final missing element is how to calculate the individual mass flows of each absorber cup from the mass flow through the whole receiver, which can be measured. To calculate the individual mass flows it has to be considered that each absorber cup has an individual orifice plate, which was optimized for a predefined flux density distribution. As no pressure state is considered and also the Reynolds number is sufficiently high enough for the considered mass flow ranges, the actual mass flow of each absorber cup is proportional to the square of the orifice diameter, i.e.

$$\dot{m} \sim d_{plate}^2 \tag{17}$$

Hence, the mass flow of one absorber cup can be calculated explicitly from the total mass flow through the whole receiver $\dot{m}_{rec}$ using the formula

$$\dot{m}_{abs,i} = \dot{m}_{rec} \cdot \frac{d_{plate,i}^2}{\sum_j^{n_{cups}} d_{plate,j}^2}. \tag{18}$$

3. Results

3.1 Test Setup

For the parametrization and validation of the receiver model, test data were recorded at the solar tower Jülich. The surface temperature and the solar flux on the receiver were measured with camera based systems [2]. The air temperatures were taken from the distributed control system.

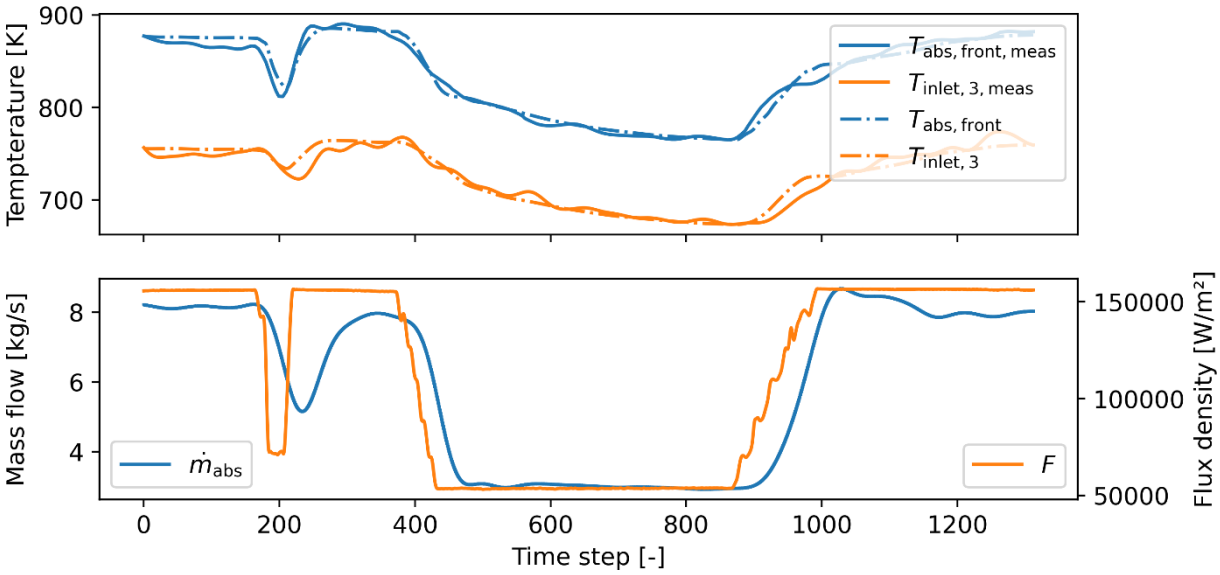


Figure 2. Results of the simulation of a single absorber cup depicting the temperature of the absorber surface and the air temperature directly behind the absorber cup.

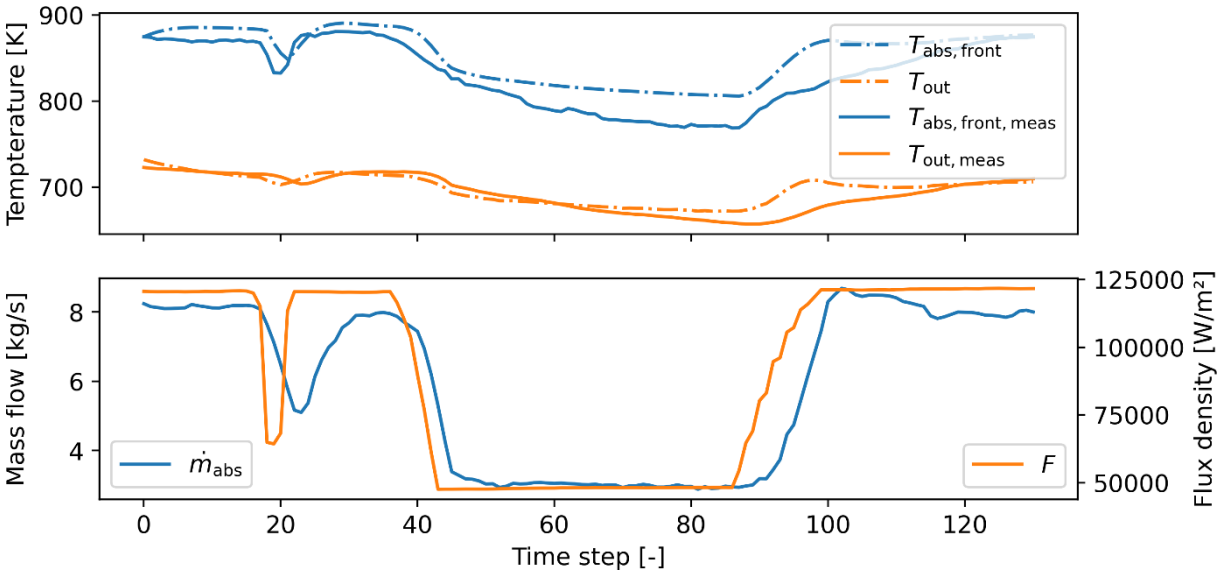


Figure 3. Results of the simulation of the whole receiver depicting the average front temperature of the absorber surface and the air temperature behind the secondary header.

The test data were recorded during a time slot with almost constant direct normal irradiation and without cloud transients. Transients were introduced by defocusing and refocusing of heliostats. The mass flow was controlled with a feedback controller using the temperature behind the secondary header.

3.2 Validation

In order to reduce modelling inaccuracies, parameters susceptible to high uncertainties are estimated using a gradient based technique starting from reasonable initial values and constrained within reasonable limits, prior to model application. At the solar tower Jülich, only a small number of absorber cups provide a temperature measurement directly behind the absorber cup that corresponds to the temperature $T_{inlet,3}$ of the introduced model. Therefore, simulations of single absorber cups as well as simulations of the whole receiver are presented.

The single absorber cup is simulated with a temporal resolution of 1 second, resulting in 1300 time steps for a time slot of about 22 minutes. The time slot starts from approximately steady state conditions at a mass flow of 8 kg/s and an air temperature of 750 K. The solar flux decreases two times for a short and a long period of time, resulting in lower temperatures and due to the mass flow controller, a decreasing mass flow.

The results of a simulation of a single cup are compared with the corresponding measurements in Fig. 2. The front temperature $T_{abs,front}$ as well as the temperature $T_{inlet,3}$ of the air directly behind the cup show good agreement. The root mean square error (rmse) of the front temperature is 6.78 K, while the rmse of the simulated air temperature is 7.51 K.

The entire receiver, consisting of 1080 absorber cups, is simulated with a temporal resolution of 10 seconds. The same time slot as before is chosen. The mean flux on the receiver surface is shown in Fig. 3, which is below the measured flux on the chosen cup in Fig. 2. The mean values of the averaged absorber cup front temperature show a significantly higher deviation between simulation and measurements. The root mean square error is 75.5 K. The air mixture temperature shows a better agreement between simulation and measurements, resulting in a root mean square error of 11.7 K.

3.3 Real Time Capability

By decoupling the dynamics of individual absorber cups, the partial differential equations for each absorber cup can be integrated individually before the resulting air mixture temperature is calculated. This way, a state observer could profit from multiple processor cores. First experiments with a moving horizon estimator showed that one absorber cup can be simulated for 10 steps in around 50 ms on an Intel Core i7-10850H. Thus, using 8 cores would result in around 6 s simulation time for the whole receiver.

4. Conclusion

The accuracy of the model is very good when simulating of a single absorber cup, but the model performs significantly worse when all receiver cups are considered. Since Fig. 2 and 3 do not show significantly different dynamics, the authors conclude that the model should be suitable for predicting the dynamics of the whole system. Reasons for the divergence are discussed below.

The parameters for the simulation of a single absorber cup are optimized only for that single cup. In contrast, the simulation of the entire receiver is performed with a constant set of parameters for all absorber cups. However, an inhomogeneous parameter set may be appropriate. The mass flow is highly inhomogeneous due to different orifice diameters in the air flow behind the absorber cup. Furthermore, the mass flow in every single absorber cup can only be approximated with Eq. 18, as there are additional flow resistances. The mass flow obviously affects the energy balances mentioned above. In addition, Tiddens et al. [4] showed that the air return ratio is mass flow dependent with respect to the entire receiver. This is likely to be true for individual absorber cups as well. Furthermore, the original design of the receiver was adopted with an external air return system to improve the performance [5]. This may also result

in inhomogeneous air return ratios regarding the location of individual absorber cups. Finally, the heat transfer coefficients are affected by the air flow, which may also result in different correction factors for the applied Nusselt correlations.

This study also aimed at developing a model of the open volumetric receiver with high spatial resolution while keeping the computational complexity low, in order to be applicable for state estimation and model predictive control. Using a moving horizon estimator with a horizon of 10 steps results in a simulation time of 6 s. This may be appropriate for non-transient scenarios and many transient cloud scenarios. However, for some fast-moving clouds, the simulation time may be too long.

5. Outlook

The authors plan to optimize the parameters of the model, which should result in mean square errors for the whole receiver being in the same range as for the single absorber cup. Furthermore, the authors plan to use the model within a moving horizon estimator for state estimation. Finally, the model will be used within an improved heliostat field control that incorporates predictions of temperature gradients on the receiver surface and respects the corresponding limits. Additionally, the performance of the open volumetric receiver could benefit from homogenous temperatures of the air leaving the absorber cups. This would reduce exergy losses due to mixing of different temperature flows and avoid unnecessarily high radiative losses. However, this temperature is not known for every single cup. The presented model allows to deduce this quantity and consider it within the control of the heliostat aimpoints.

Data availability statement

The data are not published due to legal issues. In case of interest, please consult the corresponding author (kevin.iding@dlr.de).

Author contributions

Conceptualization, methodology, formal analysis, software, investigation, writing - original draft and visualization: K.I. and D.Z.; writing - review and editing: D.M.Q.; supervision: D.M.Q and R.P.-P.

Competing interests

The authors declare that they have no competing interests.

References

1. D. Acosta, J. Garcia, M. Sanjuan, L. Oberkirsch, and P. Schwarzbözl, “Flux-feedback as a fast alternative to control groups of aiming points in molten salt power towers,” *Solar Energy*, vol. 215, pp. 12–25, doi: 10.1016/j.solener.2020.12.028.
2. M. Offergeld, M. Röger, H. Stadler, P. Gorzalka, and B. Hoffschmidt, “Flux density measurement for industrial-scale solar power towers using the reflection off the absorber,” in *SOLARPACES 2018: International Conference on Concentrating Solar Power and Chemical Energy Systems*, Casablanca, Morocco, 2019, p. 110002.
3. J. Gall, “Betriebsführung und -optimierung eines solarthermischen Turmkraftwerkes,” RWTH, IRT, Düsseldorf, 2012.

4. A. Tiddens, M. Röger, H. Stadler, and B. Hoffschmidt, “Air return ratio measurements at the solar tower Jülich using a tracer gas method,” *Solar Energy*, vol. 146, pp. 351–358, 2017, doi: 10.1016/j.solener.2017.02.027.
5. H. Stadler, A. Tiddens, P. Schwarzbözl, F. Göhring, T. Baumann, and J. Trautner, “Improved performance of open volumetric receivers by employing an external air return system,” *Solar Energy*, vol. 155, pp. 1157–1164, 2017, doi: 10.1016/j.solener.2017.07.050.